Local diagnostics to estimate density-induced sea level variations over topography and along coastlines

R. J. Bingham[1] and C. W. Hughes[2]

Received 6 May 2011; revised 9 November 2011; accepted 17 November 2011; published 21 January 2012.

[1] In the open ocean, sea level variability is primarily steric in origin. Steric sea level is given by the depth integral of the density field, raising the question of how tide gauges, which are situated in very shallow water, feel deep ocean variability. Here this question is examined in a high-resolution global ocean model. By considering a series of assumptions we show that if we wish to reconstruct coastal sea level using only local density information, then the best assumption we can make is one of no horizontal pressure gradient, and therefore no geostrophic flow, at the seafloor. Coastal sea level can then be determined using density at the ocean's floor. When attempting to discriminate between mass and volume components of sea level measured by tide gauges, the conventional approach is to take steric height at deep-ocean sites close to the tide gauges as an estimate of the steric component. We find that with steric height computed at 3000 m this approach only works well in the equatorial band of the Atlantic and Pacific eastern boundaries. In most cases the steric correction can be improved by calculating steric height closer to shore, with the best results obtained in the depth range 500–1000 m. Yet, for western boundaries, large discrepancies remain. Our results therefore suggest that on time scales up to about 5 years, and perhaps longer, the presence of boundary currents means that the conventional steric correction to tide gauges may not be valid in many places.

Citation: Bingham, R. J., and C. W. Hughes (2012), Local diagnostics to estimate density-induced sea level variations over topography and along coastlines, *J. Geophys. Res.*, *117*, C01013, doi:10.1029/2011JC007276.

1. Introduction

[2] With some records extending back over more than a century, tide gauges are a valuable tool in the study of long-term ocean and climate variability. They have, for example, been used in many studies to estimate 20th century variations in global mean sea level [e.g., *Holgate and Woodworth*, 2004; *Miller and Douglas*, 2004; *Church and White*, 2006; *Wöppelmann et al.*, 2009] as well as regional patterns of long-term sea level change [e.g., *Marcos et al.*, 2007; *Wenzel and Schröter*, 2010; *Church et al.*, 2011]. Tide gauges have also been used extensively to study interannual ocean dynamics [e.g., *Enfield and Harris*, 1995; *Hong et al.*, 2000; *Sturges and Hong*, 2001; *Firing et al.*, 2004; *Frankcombe and Dijkstra*, 2009], and as a means of validating ocean models [*Enfield and Harris*, 1995; *Tokmakian and McClean*, 2003].

[3] It is well established that in the deep ocean much of the observed variability in sea level, particularly at long periods, can be accounted for by variations in density (steric sea level), effectively assuming no variability in ocean bottom pressure [*Qiu*, 2002; *Volkov and van Aken*, 2003; *Cabanes et al.*, 2006; *Kohl and Stammer*, 2008]. In contrast, at the coast, where tide gauges are situated, the ocean's depth decreases to (effectively) zero. Hence, the steric height component of sea level, being the depth integral of density, must also vanish. In the absence of further adjustment, such a situation would create a pressure field that would lead to a depth average, along-slope geostrophic flow. Moreover, it would blind tide gauges to deep ocean variability. However, while there is evidence from satellite altimetry of a decoupling of deep and shallow water sea level variations at periods shorter than about 6 months in many regions [*Hughes and Williams*, 2010], at longer time scales deep ocean variability is evidently felt at the coast.

[4] The issue of the relationship between deep ocean steric variability and coastal sea level is material to the interpretation of tide gauge measurements. An important concern, relevant to projections of sea level rise through this century, are the relative contributions of steric expansion on the one hand, and ice sheet and glacier melting on the other. When attempting to separate out global sea level variations into their mass and density-related components, it is common to make a steric "correction" to the measurements [*Cabanes et al.*, 2001; *Miller and Douglas*, 2004]. As discussed by *Miller and Douglas* [2006], the results of this procedure can be very sensitive to where the density used in the steric correction is measured. Clearly, it cannot be a vertical section too close to the tide gauge as the water depth here will be too small to produce a significant steric signal. However,

[1]School of Civil Engineering and Geosciences, Newcastle University, Newcastle upon Tyne, UK.
[2]National Oceanography Centre, Liverpool, UK.

0148-0227/12/2011JC007276

too far away and it risks being on the wrong side of a boundary current and therefore not being relevant to sea level measured at the tide gauge. This is an issue which is still being discussed in the sea level community; our aim here is to use simple local diagnostics to clarify the issue of how deep ocean steric signals appear at the coast and to quantify the errors of a number of feasible approaches to estimating the steric driven component of coastal sea level.

[5] Consideration of these questions lead us to the more general problem of how the ocean adjusts to density changes across sloping topography; a problem which, in fact, has a long history in the context of determining velocities from density data. As recounted by *Helland-Hansen* [1934], Fridtjof Nansen, just before he died, proposed a method for determining geostrophic currents from density measurements above sloping topography. The essence of the method is to determine the dynamic height gradient between a point A lying in deep water and point B in shallower water by vertically integrating the specific volume in the usual way from an assumed zero level to the surface for point A, but for point B, integrating the density field up the sloping topography from the zero level to the point on the topography lying directly below B and then vertically to the surface. The method assumes zero velocity at the bottom.

[6] One limitation of this bottom density approach is that it neglects dynamical adjustments due to along-isobath density variations. To address this, nonlocal methods exist, in which three-dimensional density data, assumed known, is combined with the vorticity equation (neglecting nonlinear terms and adding an approximation for bottom friction) to calculate a self-consistent sea level field over some region. These methods come in two kinds: local *f* plane models [e.g., *Csanady*, 1979; *Sheng and Thompson*, 1996] which rely on sea level being provided as a boundary condition to a small region by some alternative method such as the purely local calculation, and global methods in which *f* can vary [e.g., *Greatbatch et al.*, 1991; *Myers et al.*, 1996]. These latter methods produce solutions which are sensitive to the details of the topography and require filtering or restriction to a smoother subdomain to avoid excessive noise. Interesting though these methods are, given this sensitivity and the need to integrate along convoluted contours over large distances, it is not clear how important the neglected and approximated terms are. Indeed, it may be more straightforward simply to relax a full ocean model to the observations.

[7] It would be possible, in theory at least, to pursue the approaches above to give a complete account of the factors driving coastal sea level at any particular location including the effects of local (across-isobath) and nonlocal (along-isobath) density variations. It is our intention here, however, to use local diagnostics (geostrophy and hydrostatic balance) to understand the impact topography has on the relationship between total and steric sea level variability. Our aim is to illustrate what can practically be achieved with simple, local calculations as opposed to what is effectively an inverse model of the global ocean circulation. This more realistically reflects the circumstances faced when attempting to correct a tide gauge for steric variability with limited historical observations in the vicinity of the gauge.

[8] Our analysis of the relationship between total and steric sea level in the presence of topography is based on diagnostics from a high-resolution (1/12 of a degree) global ocean model. This is sufficient resolution to produce a realistic eddy variability as well as to have multiple grid points across the steep continental slope. We demonstrate how the relationship between horizontal gradients of sea level and density is modified by the presence of topography, leading to substantial regional variations in the relationship between total and steric sea level. We show that with sufficient density information, it is possible to improve upon the current standard practice of using deep ocean steric height to correct tide gauges when estimating the mass component of sea level change.

[9] In section 2, the problem is given a mathematical formulation. Following this, in section 3, the model, and how the relevant quantities are diagnosed from it, are described. In section 4, the relationships between the gradients of these quantities are analyzed globally. The ability to reconstruct coastal sea level from density information alone is considered in section 5. The results are discussed in section 6, and conclusions are provided in section 7.

2. Mathematical Formulation

[10] We are interested in the relationship between the gradient of sea level, density and bottom pressure, so we will consider the balance of pressures

$$p_0 = p_b + p_s, \tag{1}$$

where p_0 is subsurface pressure, which is the pressure at a constant depth $z = 0$ just below the surface (and is therefore the pressure equivalent of inverse barometer–corrected sea level η', where $p_0 \approx \rho_0 g \eta'$, with ρ_0 the mean seawater density and g acceleration due to gravity). The other two terms are bottom pressure p_b and the steric pressure term:

$$p_s = -\int_{-H}^{0} \rho g \, dz, \tag{2}$$

given by an integral of the density from the seafloor ($z = -H$) to $z = 0$. Taking the horizontal gradient (∇) of (1), gives

$$\nabla p_0 = \nabla p_s + \nabla p_b = \nabla p_s + (\nabla p)_b + \rho_b g \nabla H, \tag{3}$$

where ρ_b is density at the bottom, and $(\nabla p)_b$ is the horizontal component of the three-dimensional pressure gradient, evaluated at the bottom (proportional to the geostrophic current at the bottom, rotated through 90°), in contrast to ∇p_b which is the horizontal gradient of the two-dimensional field of bottom pressure.

[11] The question we wish to address is, given density information but no bottom pressure, what is the best assumption to make in order to reconstruct the gradient of p_0 (and hence sea level) as accurately as possible. We will consider four possible assumptions, each of which makes sense in a particular context.

[12] In assumption A, $\nabla p_0 = 0$. This clearly explains none of the sea level gradient, but it is effectively the assumption being made when using an offshore steric signal to correct a tide gauge time series.

[13] For assumption B, $\nabla p_b = 0$. This is the assumption that is made when it is assumed that sea level is dominated by steric variability. In the case of a flat-bottomed ocean, it is

equivalent to assuming that the geostrophic flow is zero at the bottom, in which case it is a bottom-referenced thermal wind equation. With topography it has the effect that there can be no sea level gradient along the coast, and hence no steric effect at tide gauges.

[14] In assumption C, $(\nabla p)_b = 0$. This represents the result of a bottom-referenced thermal wind equation in the case with topography. It is the assumption that would be consistent with the presence of a node in the vertical modal current structure at the bottom of the ocean (zero geostrophic velocity at the seafloor).

[15] For assumption D, $\overline{\nabla p}^{\,z} = 0$. This assumes that the depth-averaged horizontal pressure gradient (and hence depth-averaged geostrophic current) is zero. This is equivalent to the assumption that the flow is dominated by a sum of the linear, flat-bottom baroclinic modes (modes in which the depth-integrated current is zero), with negligible contribution from the barotropic mode.

[16] In the case of assumption D, we can use hydrostatic balance (as in equations (3) and (4) of *Hughes* [2008], for example), to show that this implies that

$$\nabla p_b = -\frac{\nabla E}{H}, \tag{4}$$

where

$$E = \int_{-H}^{0} \rho g z \, dz, \tag{5}$$

or, by taking the derivative inside the integral, we can alternatively write assumption D as

$$(\nabla p)_b = -\frac{1}{H}\int_{-H}^{0} g z \nabla \rho \, dz. \tag{6}$$

Substituting each of these assumptions into (3) then gives the following sequence of approximations for the subsurface pressure gradient for assumptions A–D, respectively:

$$\begin{gathered}
\nabla p_0 \approx 0, \\
\nabla p_0 \approx \nabla p_s, \\
\nabla p_0 \approx \nabla p_s + \rho_b g \nabla H, \\
\nabla p_0 \approx \nabla p_s + \rho_b g \nabla H - \frac{1}{H}\int_{-H}^{0} g z \nabla \rho \, dz = \nabla p_s - \frac{\nabla E}{H},
\end{gathered}$$

so we can consider each of the terms, ∇p_s, $\rho_b g \nabla H$, and $-\frac{1}{H}\int_{-H}^{0} g z \nabla \rho dz$ as successive corrections to an initially estimated subsurface pressure gradient of zero. Each correction will only improve the estimate if the corresponding assumption is closer to reality than the previous assumption. By taking ∇p_s to the left-hand side, approximations B, C and D can also be seen as successive approximations to ∇p_b. The final term, added in D, represents minus the depth average of the pressure gradient which would be calculated by integrating horizontal density gradients up from the bottom, and can be thought of as the addition of a depth-independent current to ensure that the depth-averaged current (rather than bottom current) is zero.

[17] In fact, C is simply understood as a generalization of the hydrostatic calculation of steric sea level above some seafloor position H_0 at which bottom pressure variability is assumed to be negligible (later we choose the 3000 m depth contour as our reference). The generalization, rather than integrating along a vertical line, takes a slanting path along the seafloor from the H_0 contour to the coast. The prediction at the tide gauge is then given by

$$p_0 = -\int_{H_0}^{\text{coast}} \rho_b g \, dz. \tag{7}$$

This is precisely the bottom integral method as employed by *Helland-Hansen* [1934] in the context of determining slope currents, and is equivalent to a thermal wind calculation referenced to the seafloor.

[18] Note that we are considering these approximations to ∇p_0 as local. If we take the curl of each of the approximate balances, we can see that assumptions C and D can only be valid globally if bottom density (in the case of C), or E (in the case of D) is a function of ocean depth only. Otherwise, estimates of sea level differences between two points, based on an integral of the corresponding equation, will be path dependent. This observation is the motivation behind the nonlocal methods described earlier [*Csanady*, 1979; *Sheng and Thompson*, 1996; *Greatbatch et al.*, 1991; *Myers et al.*, 1996], which effectively add an assumed geostrophic bottom velocity chosen to make the integral path independent.

3. Model Diagnostics

[19] The main results of this paper are based on an analysis of the Ocean Circulation and Climate Advanced Modeling project model (OCCAM) run at the National Oceanography Centre, Southampton. OCCAM is a global, z-level, free surface model with a rotated grid over the North Atlantic, and is forced with NCEP reanalysis products. Freshwater fluxes, including evaporation minus precipitation and river runoff, are explicitly represented in the model and included in the free surface computation. The model includes a coupled sea ice component and employs a partial bottom cell scheme for a more faithful representation of bottom topography. The run we are considering (run 401) is at 1/12 of a degree horizontal resolution, with 66 vertical levels, and covers the 20 year period 1985–2004, following an initial 4 years of spin-up. Monthly mean fields for the 19 year period 1986–2004 were used for the analysis presented here. Further details of the model formulation are given by *Marsh et al.* [2009].

[20] Sea level is obtained directly from the model. Since the model has a free surface, the sea level includes variations due to atmospheric loading. These are removed, to give dynamic sea level, by making the inverted barometer correction. Dynamically irrelevant (because no horizontal pressure gradients arise) global mean sea level changes due to mass fluxes in to or out of the ocean are also removed by subtracting the global mean sea level at each time step. Steric height is determined by the vertical integration of density, which is computed from the potential temperature and salinity fields output by the model. Because OCCAM is a Boussinesq model that conserves volume rather than mass, following *Greatbatch* [1994], the global mean sea level is set equal to the global mean steric sea level (calculated from an integral of density over the entire ocean volume), by adding a spatially constant value at each time step. This ensures that

the total ocean mass is conserved (global mean sea level changes are purely steric). Bottom pressure (as equivalent water thickness) is then given by subtracting steric height from the sea level. The time mean is removed from all fields, and the time series are detrended, leaving time series of anomalous sea level, etc. These three height fields are then scaled by $g\rho_0$ to obtain the subsurface pressure p_0, the steric pressure p_s, and the bottom pressure p_b. Horizontal gradients of these quantities are then calculated using a first-order forward difference scheme.

[21] The bottom density term $\rho_b g \nabla H$, appearing first in approximation C, is determined by computing the density on the vertical wall of a step (or the average density, if a step extends over more than one model layer) and multiplying this by the gradient of the step. Steps are defined by the model topography according to the first-order forward difference scheme. Since, in the discrete model domain, the height of a step, and therefore what constitutes the bottom density, may be different in the zonal and meridional directions, we compute the x and y components of this field separately. Obviously, $\rho_b g \nabla H$ is zero where the seafloor is flat.

[22] To calculate the depth average density term $-\frac{1}{H}\int_{-H}^{0} gz\nabla\rho dz$ appearing in approximation D we first calculate the full-depth potential energy from the model density, and the potential energy gradient is computed using the first-order forward difference scheme. The potential energy E is then scaled by the total depth as in approximation D, and the bottom density defined above is subtracted to give the required depth average density term. Finally, for both density terms the long-term time mean and trend are removed.

4. Gradient Analysis

[23] Following the formalism developed in section 2, we now consider the relationship between the horizontal gradients of subsurface pressure ∇p_0 (sea level) and its steric ∇p_s and bottom pressure ∇p_b components. Of particular interest, is how the relationship between these quantities depends on topography (this is crucial for understanding the dynamics of coastal sea level). To examine the variability of these vector quantities we define the metric K, which is analogous to the square root of time mean eddy kinetic energy:

$$K(\mathbf{a}) = \sqrt{\frac{\langle a_1 \rangle + \langle a_2 \rangle}{2}}, \tag{8}$$

where $\mathbf{a} = (a_1, a_2)$ denotes a vector field and $\langle a_* \rangle$ represents the temporal variance of each vector component. To quantify the *skill* with which a vector $\mathbf{b}$ approximates another $\mathbf{a}$, we define vector skill as

$$S(\mathbf{a}\|\mathbf{b}) = 1 - \frac{\langle a_1 - b_1 \rangle + \langle a_2 - b_2 \rangle}{\langle a_1 \rangle + \langle a_2 \rangle}. \tag{9}$$

This is a measure of the fraction of the variance in vector $\mathbf{a}$ that is accounted for by vector $\mathbf{b}$.

[24] Figure 1a shows elevated ∇p_0 variability in regions of strong, unstable currents such as the western boundary currents and the Antarctic Circumpolar Current. It is also clear that ∇p_0 variability is frequently much weaker where the ocean is shallow, meaning assumption A may be reasonable in these regions. However, the strong variability seen immediately off the continental shelf demonstrates, unsurprisingly, that assumption A is not generally tenable. It therefore raises questions as to the validity of the steric correction that is commonly applied to tide gauges.

[25] Turning to the map of $K(\nabla p_s)$ (Figure 1b) we find there is little to distinguish it from the corresponding map for ∇p_0, indicating that steric variability is the dominant driver of ∇p_0 for the time scales considered (i.e., monthly to interannual). This is confirmed by Figure 1c which shows the skill of ∇p_s in accounting for the variance of ∇p_0. Close inspection of Figure 1c, however, reveals that this close link tends to break down in coastal regions around both continental landmasses and small mid-ocean islands. Nonetheless, in relation to our approximations given above, we can say with confidence that approximation B is reasonable over the vast majority of the global ocean's extent.

[26] The veracity of assumption B, which states that ∇p_b is zero, is directly examined in Figure 2a. As expected from Figure 1, the variability of ∇p_b is generally much weaker than is the case for ∇p_0 or ∇p_s. In the open ocean, heightened ∇p_b variability is found in the regions of the strongest currents where barotropic eddy variability is generated, most notably in the Gulf Stream and Antarctic Circumpolar Current. Yet, as Figure 1c shows, the magnitude of this variability is too small to significantly degrade the close link between ∇p_0 and ∇p_s (at the time scales considered). At this point the reader is encouraged to inspect the electronic form of Figure 2a at large zoom (400% if possible). Viewed in this way, a close relationship between ∇p_b and topography is revealed: The magnitude of ∇p_b variability is elevated where the topography is steepest. In fact, over steep topography the magnitude of ∇p_b generally exceeds that of ∇p_0. Since, by equation (3), ∇p_0 is the sum of ∇p_s and ∇p_b, the corollary of this is that the magnitude of ∇p_s over steep topography will also exceed that of ∇p_0 but the variations will be of opposite sign to ∇p_b.

[27] By taking the steric term to the left hand side, approximation C implies that ∇p_b can be approximated by the topographic density term $\rho_b g \nabla H$. The validity of this approximation is tested in Figure 2b (again, best viewed in electronic form) where K is mapped for the residual $\nabla p_b - \rho_b g \nabla H = (\nabla p)_b$. (We shall refer to this as the first-order residual of ∇p_b.) While the regions of elevated ∇p_b variability (Figure 2a) in the open ocean are undiminished in $(\nabla p)_b$, nearly all of the variability over steep topography has been removed. The fact that at the time scales considered, the topographic density term is the primary determinant of ∇p_b over steep topography, is further confirmed by the vector skill mapped in Figure 2c. Almost anywhere that steeply sloping topography is found, the bottom density term accounts for nearly all of the ∇p_b variability. This topographic influence is not only confined to the continental slopes, but is also seen in the interior, where the seafloor relief, including such features as the Mid Atlantic Ridge and associated fractures, leave their imprint in ∇p_b.

[28] Finally, we consider approximation D in the sequence, which adds a final depth average pressure gradient term to the approximation of the sea level gradient. The usefulness of this additional term is tested in Figure 3a where K is mapped

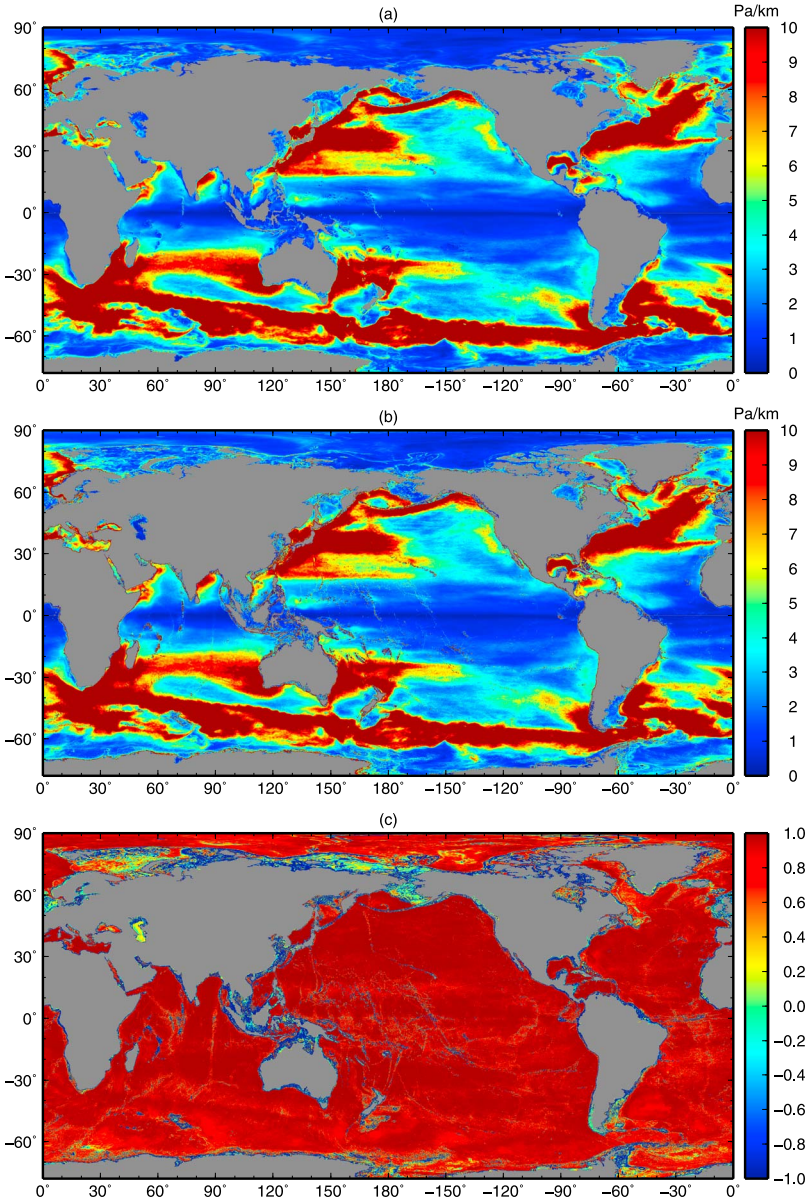

Figure 1. (a) The square root of the mean vector variance (K as defined in the text) of the subsurface pressure gradient ∇p_0. (b) The square root of the mean vector variance of steric pressure gradient ∇p_s. (c) The vector skill (S as defined in the text) of the steric pressure gradient in accounting for the total subsurface pressure gradient. A skill score of 1 corresponds to perfect agreement.

for the second-order residual $\nabla p_b - \rho_b g \nabla H - (-\frac{1}{H}\int_{-H}^{0} gz\nabla\rho\, dz) = \overline{\nabla p}^{z}$. Over quiet regions of the ocean, this final correction does account for some of the residual $(\nabla p)_b$ variability, as indicated by the somewhat smoother map of K for $\overline{\nabla p}^{z}$. This "tidying up" effect is made clearer in Figure 3b, which shows the skill of the depth average pressure gradient term in accounting for the variance in $(\nabla p)_b$. In particular, we see that depth-averaged pressure gradient term dominates ∇p_b variability in the tropics. It also seems to be important around Antarctica, to the south of the ACC, and also in some parts of the Arctic ocean. Returning to Figure 3a, we see that for regions of high ∇p_b variability in the deep ocean, removal of the depth average pressure gradient term actually adds to, rather the reduces, the total variability. For these regions, approximation C is superior to approximation D.

[29] Figure 4 summarizes of the quality of each successive approximation to the subsurface pressure gradient as a function of depth (Figure 4a) and topographic gradient (Figure 4b). The depth averaged K for ∇p_0 (blue) again confirms that assumption A is not generally tenable, even though K does decrease by more than a factor of two between its maximum in the 2500–3000 m depth range and its minimum in the shallowest 500 m. In contrast, the steepness of the topography has little influence on ∇p_0 (Figure 4b).

[30] If approximation B is valid, then the depth average of $K(\nabla p_b)$ (red) should be close to zero, or at least much smaller than the depth average of $K(\nabla p_0)$ (blue). Yet, while this is certainly true of the deep ocean, where $K(\nabla p_b)$ is a

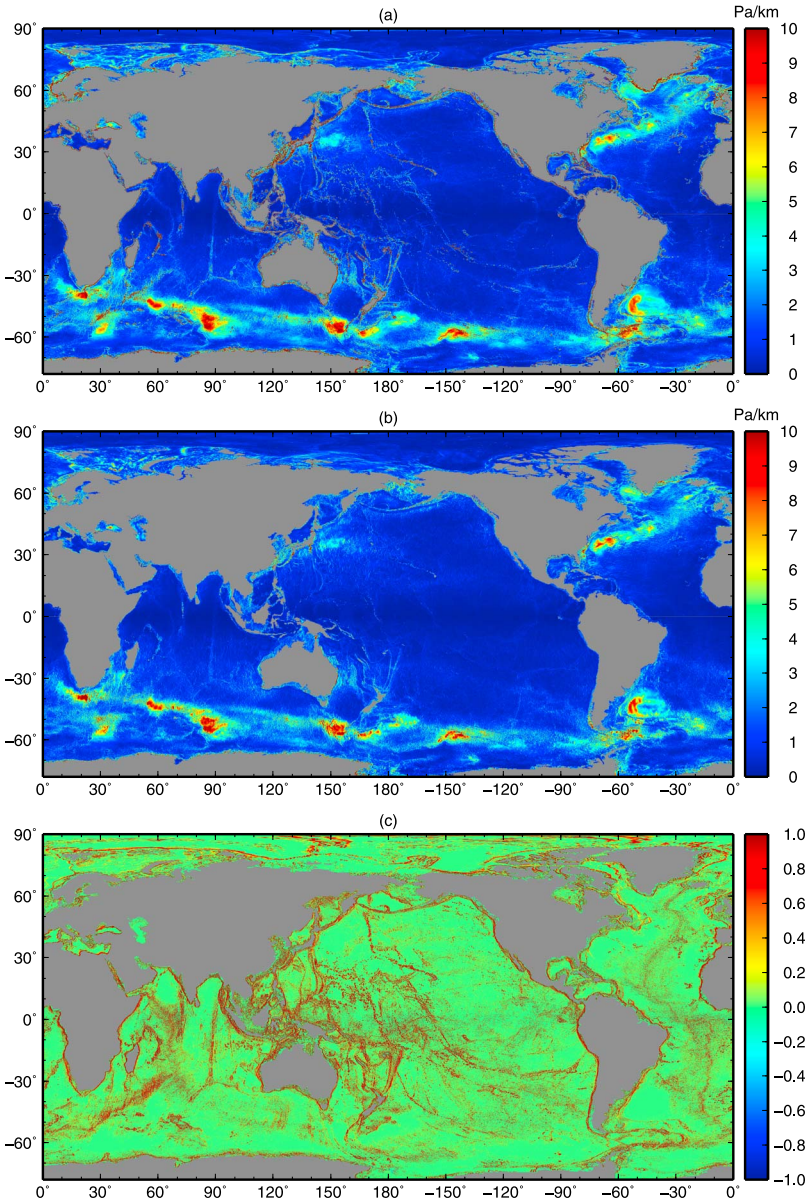

Figure 2. The square root of the mean vector variance (K as defined in the text) of the two successive reductions of the subsurface pressure gradient, corresponding to the terms assumed to be zero in assumptions B and C in the text: (a) The steric pressure term removed to give the bottom pressure gradient. (b) As in Figure 2a, but with the topographic density term also removed to give the horizontal pressure gradient at the ocean floor. (c) The vector skill (S as defined in the text) of the topographic term in accounting for the bottom pressure gradient.

factor of 5 smaller than $K(\nabla p_0)$, the fidelity of the approximation exponentially declines as we move to shallower waters, such that in the upper 500 m interval the average ∇p_b variability is in fact more than twice that of ∇p_0. Where this is the case, it means that variations in both ∇p_s and ∇p_b are greater than the variations in ∇p_0. They are, however, out of phase, such that, to a large extent, they negate each other in the sum. This out-of-phase, compensatory nature of the steric and bottom pressure gradients is even clearer when we compute averages of K over topographic gradient intervals (Figure 4b). As the steepness of the topography increases, so too does the amplitude of ∇p_b, and therefore, since ∇p_0 does not change, so to must the compensatory ∇p_s amplitude increase. It is because of this strong compensation between the steric and bottom pressure components of the subsurface pressure gradient, that the steepness of the topography does not leave its imprint in ∇p_0. To put it another way, density changes with no horizontal gradient produce no sea level gradient. But the intersection of such density changes with topography produces compensating steric sea level and bottom pressure gradients.

[31] For approximation C to hold, the first-order residual $(\nabla p)_b$ (green) must be close to zero. Figure 4a we see that the fraction of ∇p_b variability accounted for by the topographic term depends strongly on depth, accounting for more than 60% of the ∇p_b variability in the upper 500 m,

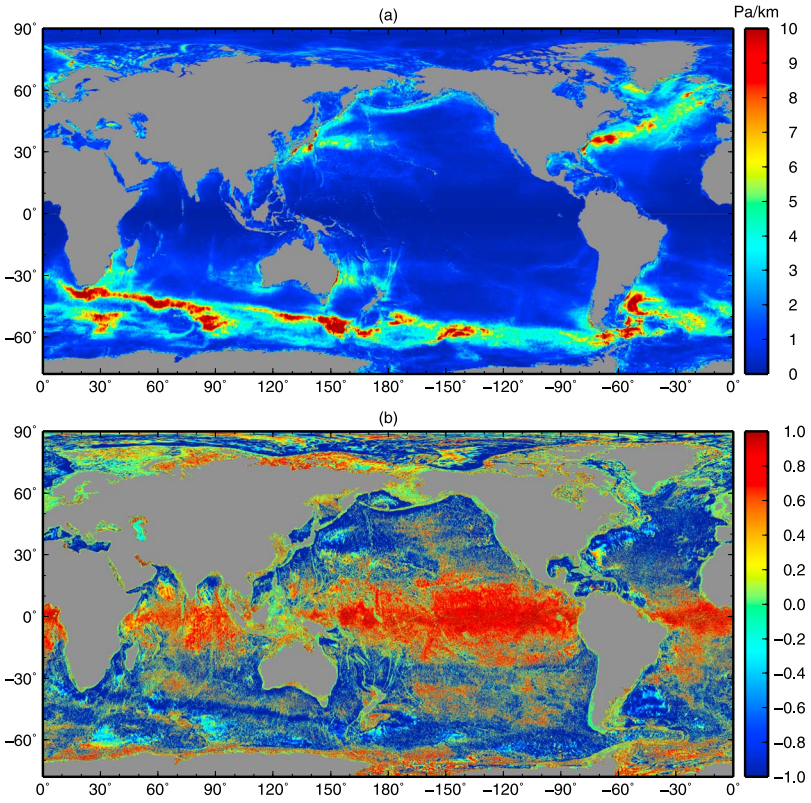

Figure 3. (a) As in Figure 2b, but with the depth averaged density gradient term also removed. (b) The vector skill (S as defined in the text) of the depth average density term in accounting for the bottom pressure gradient less the topographic term.

but very little below 2500 m. An even stronger relationship is found when considered in terms of topographic gradient, with the topographic density term accounting for most of the ∇p_b variance for all but the lowest topographic gradient ranges.

[32] Finally, approximation D effectively states that the second-order residual $\overline{\nabla p}^{\,z}$ (yellow) is close to zero. For all depth intervals, except the upper 500 m interval, and for all topographic gradient intervals, we see that subtraction of the depth average density term actual increases the variability of the second-order residual. So although, as Figure 3 showed, the depth average density term does account for some of the remaining ∇p_b variability, this is outweighed by the other, more energetic regions where subtraction of the depth average density term adds to the total variability.

5. Reconstructing Coastal Sea Level

[33] So far we have considered the relationship between total and steric sea level in the presence of topography wherever it occurs, but our primary motivation is to understand how open ocean and coastal sea level are related. The analysis of section 4 was framed in terms of the gradients of (essentially) sea level and its components, but here our interest lies in the actual sea level variability at the coast, and, in particular, how well coastal sea level can be reconstructed under the assumptions given above. That is, using local diagnostics, rather than a globally consistent approach that includes along-isobath density variations.

[34] Coastal sea level obtained from any of the approximations A–D given above has the very general form

$$h(\mathbf{x_C}) \approx F(\mathbf{x_D}, \rho, H) + (\rho_0 g)^{-1} p_b(\mathbf{x_D}), \tag{10}$$

where $\mathbf{x_C}$ is the coastal position and $\mathbf{x_D}$ is some deep ocean position. On the right hand side of this approximation the first term can be determined entirely from density shoreward of $\mathbf{x_D}$, while the second term represents an external boundary condition, which can be minimized by taking $\mathbf{x_D}$ sufficiently far offshore. On the basis of a number of studies [e.g., *Vinogradova et al.*, 2007; *Bingham and Hughes*, 2008], here we take this to correspond to a depth of 3000 m.

[35] To reconstruct coastal sea level we would ideally wish to choose $\mathbf{x_D}$ such that the path between $\mathbf{x_C}$ and $\mathbf{x_D}$ intersected the continental slope and shelf perpendicularly. To approximate this in the model domain we take $\mathbf{x_D}$ to be the closest model grid point with a depth of least 3000 m that can be connected to $\mathbf{x_C}$ by a great circle path that does not intersect land grid points. (As a result of this last condition, for a small number of coastal grid points, semienclosed by land, a deep ocean partner cannot be found.) The gradient field is then integrated along the (discretized) straight line joining $\mathbf{x_D}$ and $\mathbf{x_C}$. This procedure is, in fact, only necessary for approximations C and D. In (10), $F = (\rho_0 g)^{-1} p_s(\mathbf{x_D})$ for assumption A, and so, assuming that $p_b(\mathbf{x_D}) = 0$ we simply take steric sea level at $\mathbf{x_D}$ as the approximation to coastal sea level. This is equivalent to the steric correction usually used to correct tide gauges. We do not consider approximation B

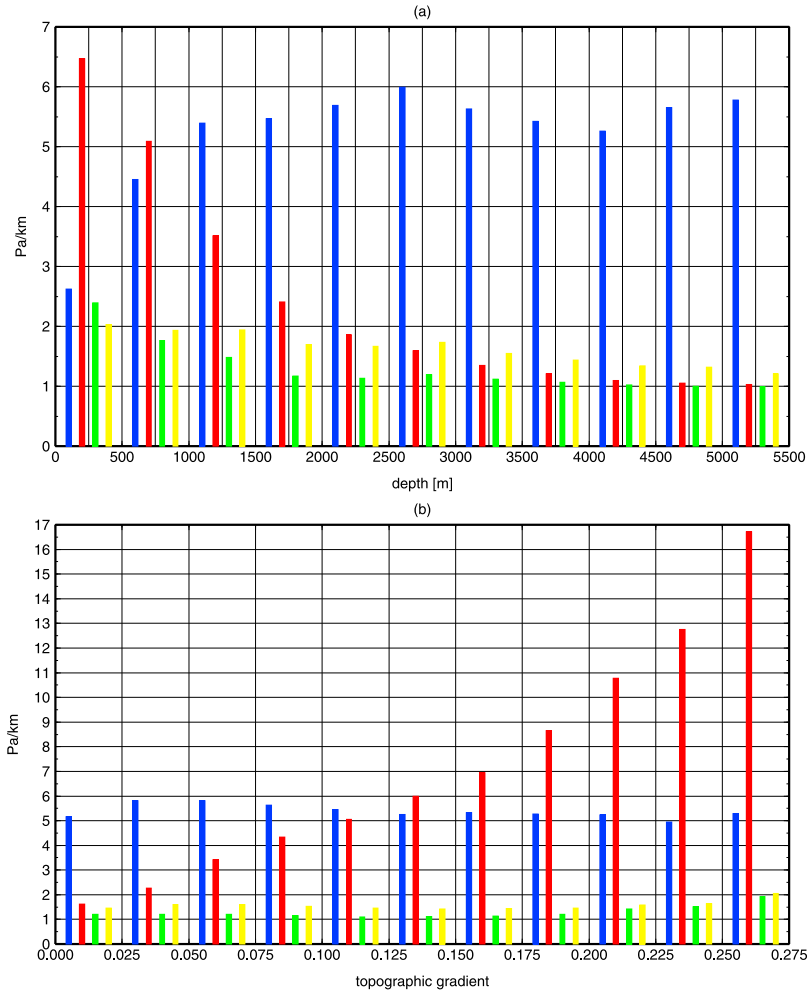

Figure 4. (a) The square root of the mean vector variance (K as defined in the text) of the subsurface pressure (sea level) gradient averaged over 500 m depth intervals (blue). Subsequent bars represent averaged K of the subsurface pressure gradient residual upon cumulative subtraction of the steric pressure gradient (red; assumption B), the topographic density term (green; assumption C), and the depth average density gradient term (yellow; assumption D). (b) As in Figure 4a, but with averages computed over intervals of the topographic gradient. Averages are computed over the ranges that bracket the vertical bars.

further because we already know that at the coast, where the depth is zero, steric height alone cannot account for coastal sea level variability.

[36] As the characteristics of the sea level variability on the eastern and western boundaries are rather different, we first consider the eastern boundaries of the Atlantic and Pacific before progressing to consider their western boundaries. These boundaries are marked in Figure 5, with annotated latitudes in subsequent along-shore plots marked.

5.1. Eastern Boundaries

[37] The coastal sea level anomaly for the Atlantic eastern boundary from 35°S to 50°N is shown in Figure 6a (and in Figure 7a for the Pacific eastern boundary). Because the seasonal cycle dominates the coastal sea level variability, it is removed and displayed separately in Figure 6 (left). The remaining signal is low-pass filtered with a 7 month boxcar filter to remove high-frequency variability and the results are shown in Figure 6 (right). While certainly interesting, it is not our intention here to give a full account of the temporal and latitudinal form of the sea level variability itself.

[38] Figure 6b shows that the deep ocean steric height does account for much of the seasonal cycle in coastal sea level along the Atlantic eastern boundary. For the lower-frequency variability, however, the steric approach only works well for latitudes from about 5°S to 12°N. Beyond this equatorial band, coastal sea level becomes progressively decoupled from the deep ocean steric signal, with a narrow band of especially poor correspondence between 33°N–38°N near to the Strait of Gibraltar. Comparing this with the reconstruction based on approximation C (Figure 6c), shows that the bottom density approach is generally more successful than the steric method in accounting for coastal sea level variability, both seasonal and interannual.

[39] For the interannual component, the skill (given by the scalar analog of (9)) of the steric and bottom density methods in accounting for coastal sea level is quantified in Figure 8. With the exception of a few isolated latitudes, the

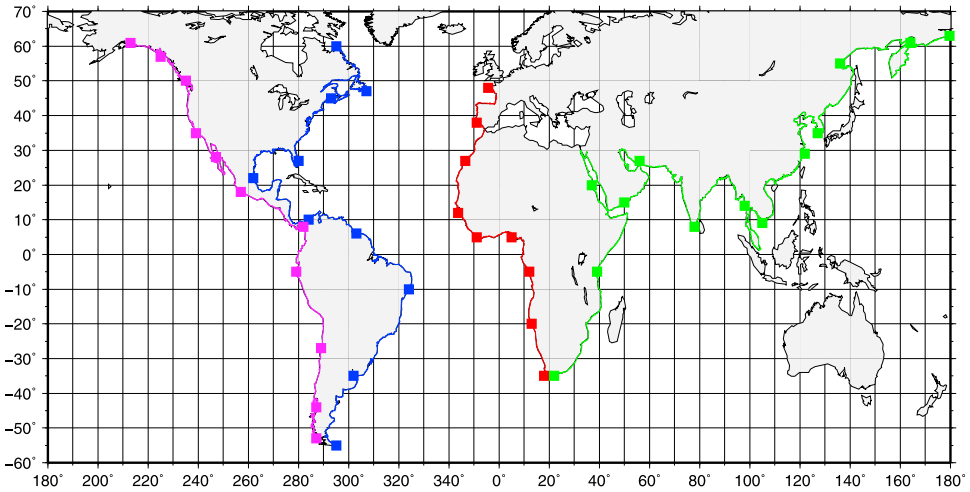

Figure 5. A map showing the coastlines along which sea level and related quantities are plotted in Figures 6, 7, 10, and 11. Squares correspond to the latitudes annotated in Figures 6, 7, 10, and 11.

bottom density method accounts for more of the variance than does the steric method, with the difference becoming more pronounced at higher latitudes. This is especially true of the Southern Hemisphere, where the skill of the steric method drops rapidly south of about 15°S, while the skill of the bottom density method remains high. In the Northern Hemisphere, the skill of both methods diminishes toward the pole, but for the bottom density method it does so less rapidly than for the steric method. The hemispheric asymmetry most likely reflects somewhat different dynamical regimes of the North and South Atlantic.

[40] If we limit ourselves to considering only basin scale fluctuations in sea level by forming along-shore means for southern (35°S–5°S), equatorial (5°S–10°N), northern (10°N–

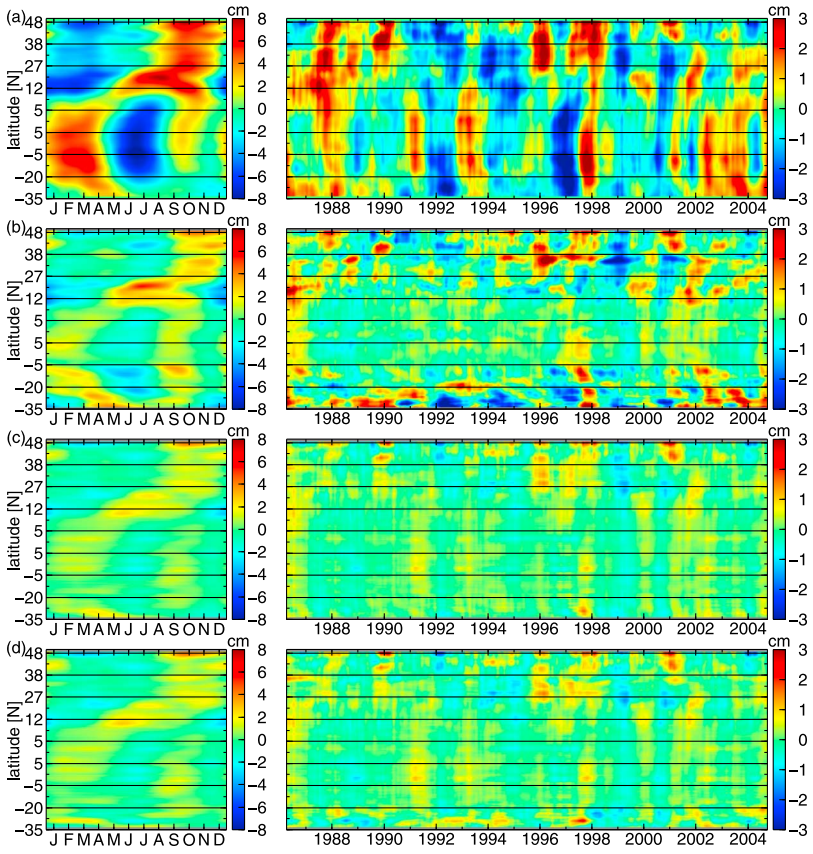

Figure 6. (a) Modeled coastal sea level variability along the eastern boundary of the Atlantic. (b–d) Residuals upon subtraction from the sea level shown in Figure 6a of the reconstructions of coastal sea level under approximations A, C, and D, respectively.

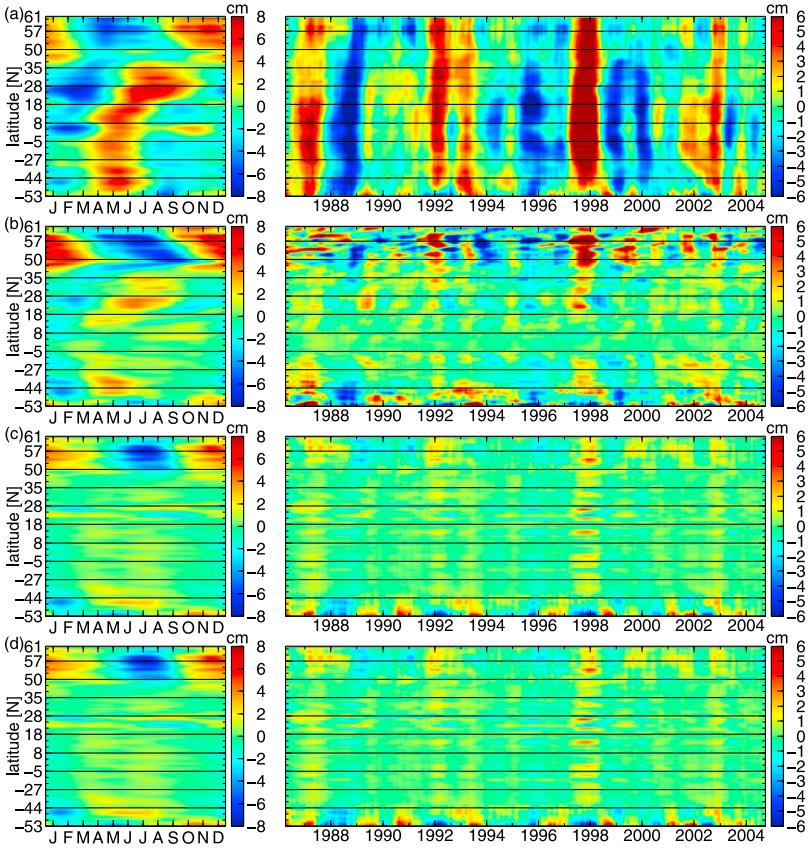

Figure 7. (a) Modeled coastal sea level variability along the eastern boundary of the Pacific. (b–d) Residuals upon subtraction from the sea level shown in Figure 7a of the reconstructions of coastal sea level under approximations A, C, and D, respectively.

50°N) domains of the Atlantic eastern boundary (Figure 9a), then we find that the differences between the steric and bottom density methods for the eastern Atlantic boundary are less marked. This suggests that the differences between the two methods tend to arise from localized variability. For the equatorial domain, the skill of the steric method is 91%, while for the bottom density method it is 95%. For the southern domain the advantage of the bottom density method (skill 96%) over the steric method (skill 76%) is more noticeable. Here the steric method gets the timing of the fluctuations correct but underestimates their amplitude, leading to a peak-to-peak error of more than 1 cm for the large 1997/1998 fluctuation. The same is true of the northern domain, but because the bottom density method also tends to underestimate the amplitude of the fluctuations, here the difference between the two methods is less pronounced (the steric method has skill 81%, while for the bottom density method it is 92%).

[41] A similar picture emerges for the eastern boundary of the Pacific. The steric method (Figure 7b) is successful in the equatorial band (5°S to 18°N), but becomes progressively poorer with increasing latitude. This in spite of the fact some of the variability at high latitudes is clearly part of a meridionally coherent mode; for example, the sea level high associated with the 1997/1998 El Niño. The steric approach is better at accounting for the seasonal cycle, apart from latitudes above 50°N where the residual is of a similar magnitude to the original signal. For all latitudes outside of the equatorial band, the bottom density method (Figure 7c) is more successful than the steric method at recovering the coastal sea level signal, with the improvement increasing with latitude. The seasonal sea level cycle is also reconstructed more faithfully. Again, apart from a few isolated latitudes, the skill of the bottom density method is greater than that of the steric method (Figure 8b). In the Southern Hemisphere, the skill of the steric method begins to drop off rapidly south of about 32°S, while for the bottom density method the dropoff begins at 42°S. Forming along-shore mean time series (Figure 9b) for the South Pacific between 57–40°S, we find that this difference in dropoff latitude translates into a somewhat closer match between the actual and bottom density mean time series (skill 78%), as compared with the steric method (skill 49%) which tends to underestimate the amplitude of the fluctuations. In contrast, for a wide band straddling the equator (40°S–32°N), the along-shore mean time series are, as they were in the Atlantic (but in that case over a smaller latitude range), almost indistinguishable (a skill of 98% for the steric method and 99% for the bottom density method). In the Northern Hemisphere, the skill of the steric method begins to fall off at 30°N and fluctuates around zero north of 48°N. The skill of the bottom density method also decreases toward higher latitudes, but much less so, and is still above 60% at 60°N. Eliminating local effects by forming an along-shore mean between 32°N–61°N, we find that of all the eastern boundary time series considered, here the superiority of the bottom density method is most

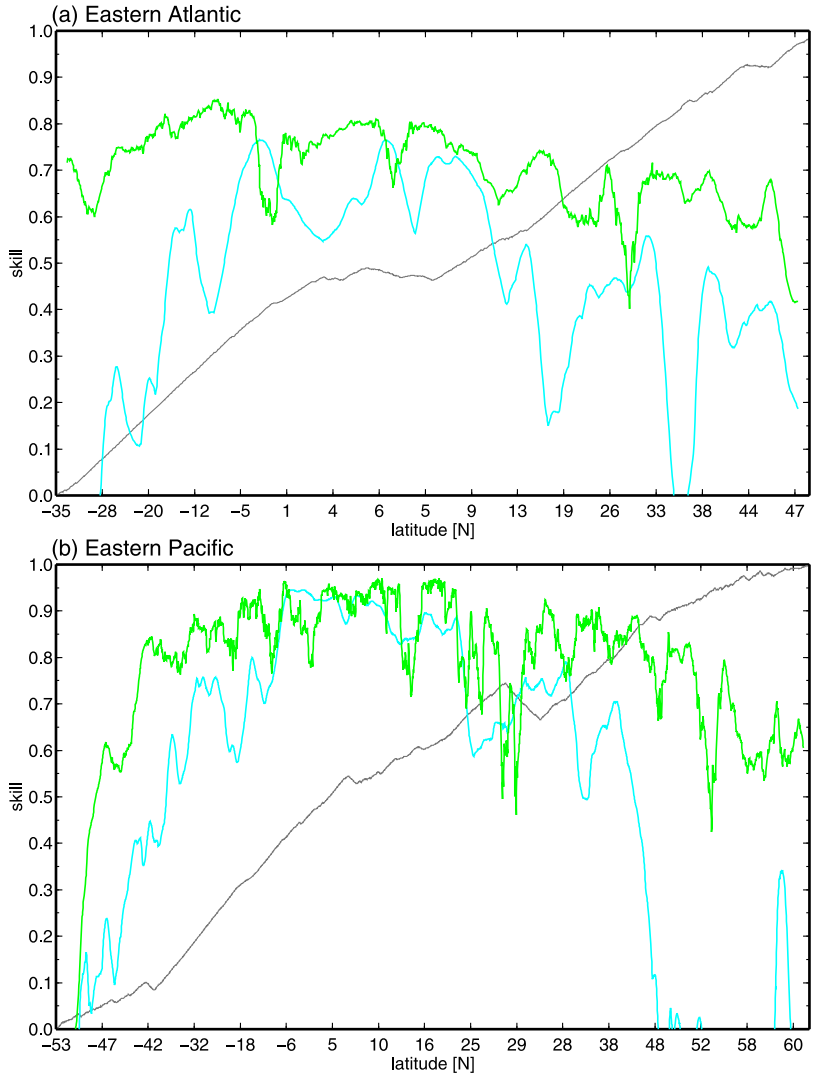

Figure 8. (a) The skill of approximations A (cyan) and C (green) in accounting for the modeled coastal sea level variability along the Atlantic eastern boundary. (b) The same as Figure 8a for the Pacific eastern boundary. The grey line gives an indication of how latitude varies along the coast between the latitudes marked on the *x* axis.

pronounced. The bottom density time series (skill 93%) closely follows the sea level time series, whereas the steric method reconstruction (skill 38%) follows it only approximately, and perhaps with a few months lag.

[42] Finally, for the eastern boundaries, we consider the difference the additional depth average pressure gradient term in approximation D makes to our ability to reconstruct coastal sea level. From earlier results we can expect this difference to be negligible, an expectation confirmed for the eastern boundaries of the Atlantic and Pacific in Figures 6d and 7d. This shows that for the ocean eastern boundaries the depth averaged, bottom referenced pressure gradient is small in comparison to the topographic density term.

5.2. Western Boundaries

[43] The dynamical regimes of western boundaries are generally more complicated. Therefore, we can expect the reconstruction of coastal sea level using only density information to be more challenging here. Focusing first on the Atlantic western boundary from 55°S to 60°N (Figure 10; Figure 11 shows the Indian and Pacific western boundaries), this is indeed what we find. While on the Atlantic eastern boundary, the steric method accounts for at least some of the sea level variability, on the Atlantic western boundary it is clear that with the exception of a few small stretches of coastline at low latitudes, the deep ocean steric height is a poor approximation to coastal sea level (Figures 10a and 10b). Overall, the deep steric signal tends to be much larger than the coastal sea level and so its subtraction adds to, rather than reduces, the coastal sea level variance. This is true of both the seasonal and lower-frequency variability. For this reason, the skill of the steric method along most of the Atlantic western boundary is negative. Only for some isolated latitudes near the equator does the skill exceed 50% (see Figure 12a).

[44] The bottom density approach generally results in a more accurate reconstruction of coastal sea level along the Atlantic western boundary, both for the seasonal and

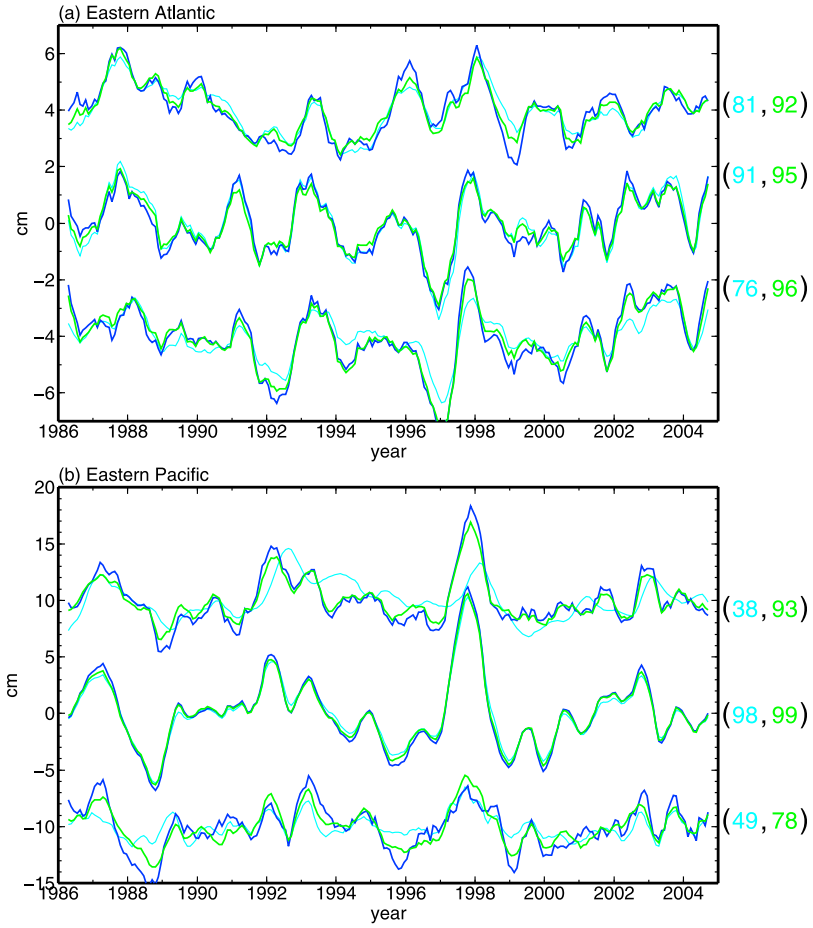

Figure 9. (a) Averages along the Atlantic eastern boundary of coastal sea level (blue) and sea level reconstructions based on assumption A (cyan) and assumption C (green). Averages are computed over 35°S–5°S (bottom), 5°S–10°N (middle), and 10°N–50°N (top). (b) The same as Figure 9a for the Pacific eastern boundary, with averages computed over 57°S–40°S (bottom), 40°S–32°N (middle), and 32°N–61°N (top). The skill scores for the two reconstructions are shown to the right of each along-shore mean time series in corresponding colors.

interannual components (Figure 10c). Along nearly the entire length of this coastline, unlike the steric method reconstruction, the residual upon subtracting the bottom density reconstruction from the actual sea level is smaller than the sea level itself. Two conclusions can be drawn from this: First, the bottom density method does a much better job than the steric approach in reconstructing the density-related component of coastal sea level. Second, there are other processes, however, that contribute to the coastal sea level variability, which, for some stretches of coasts, are much greater than the density related signal. The superiority of the bottom density method is demonstrated by the much higher skill scores obtained by this approach compared with the scores obtained by the steric method (Figure 12a). Within about 35° of the equator, with the exception of on the equator itself, the bottom density method generally accounts for more than half of the interannual variance. At higher latitudes, the skill of the bottom density method is lower, and for some latitudes even negative. Note, the skill of both the steric and bottom density methods on the western boundary is not as good as for the eastern boundary, but the superiority of the bottom density method over the steric method is generally much greater on the western boundary.

[45] As we did for the eastern boundaries, we look at the reconstructions on the basin scale by forming along-shore averages for the South Atlantic domain (55°S–10°S), the equatorial domain (10°S–20°N) and the North Atlantic domain (37°N–50°N) (Figure 13a). Even at these scales, and for all domains, the bottom density reconstructions come much closer than the steric method estimates to the actual sea level time series. For the South Atlantic domain, the bottom density method gets most of the long-term variability correct, but underestimates the amplitude of some of the interannual fluctuations (skill 66%). In contrast, the steric method bears little resemblance to the actual coastal sea level (negative skill). A similar picture is found for the North Atlantic domain, but with even greater errors in the steric approach (negative skill compared with 52% for the bottom density method). For the equatorial bands of the eastern boundaries, the two approaches are almost identical, both capturing nearly all of the coastal sea level signal. However, on the Atlantic western boundary, while the bottom density method clearly recovers most of the equatorial coastal sea

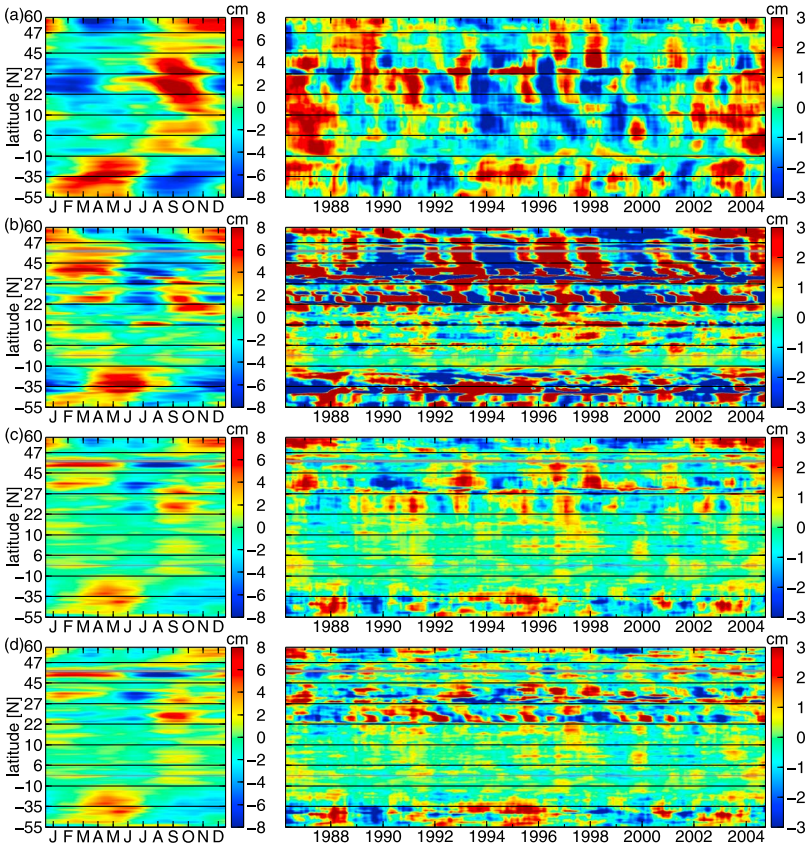

Figure 10. (a) Modeled coastal sea level variability along the western boundary of the Atlantic. (b–d) Residuals upon subtraction from the sea level shown in Figure 10a of the reconstructions of coastal sea level under approximations A, C, and D, respectively.

level variability (skill 91%), the steric method does not (skill 12%).

[46] As was the case for the eastern boundaries, the additional refinement of assumption D, makes little difference to the sea level reconstruction (Figure 10d). In fact, between 22°N and 45°N, the reconstruction is poorer than that for the bottom density method, consistent with a significant depth-average flow above the continental slope at these latitudes.

[47] Along the western boundaries of the Indian and Pacific oceans a similar picture emerges (Figure 11). In most places the deep steric signal is larger than the coastal sea level and so errors in the steric reconstruction often exceed the coastal sea level signal itself. In contrast, the bottom density reconstruction gives a much more accurate estimate of the coastal sea level. Again, the additional refinement of approximation D does little to improve upon the bottom density method, and, in fact, decreases the fidelity of the reconstruction somewhat. Figure 12b, confirms that the bottom density method reconstruction captures much more of the interannual coastal sea level variability than does the steric method.

[48] Forming along-shore mean time series (Figures 13b), we find that along the western boundary of the Indian Ocean (35°S–5°S) there is good agreement between the actual sea level and the bottom density reconstruction (skill 93%). In contrast, the agreement with the steric reconstruction is poor (negative skill). While there is some agreement in the timing of the steric method fluctuations, their amplitudes are too large. Moving to the Pacific, the first time series encompasses the coastline from Singapore to 30°N. Here the bottom density method follows closely the actual sea level time series (skill 89%), while the steric method time series bears little resemblance to the actual sea level (negative skill). The second interval extends from 30°N–53°N. Here, again, the bottom density reconstruction is in much better agreement with the actual sea level (skill 54%) than is the steric reconstruction (negative skill), with the fluctuations in the steric sea level much larger than the coastal sea level variability. Finally, for the most northerly interval (53°N–63°N) the bottom density reconstruction (skill 89%) is much closer to the truth than the steric method (negative skill).

5.3. The Effect of Reference Depth on the Steric Correction

[49] In the preceding analysis we have taken 3000 m as the common reference depth for both the steric and bottom density methods. This is because, as described above, it can safely be assumed that the bottom pressure component of sea level is small at 3000 m. Also, taking a common reference is useful in the comparison of local dynamic balances on the slope. Furthermore, from an observational perspective 3000 m is an optimistic depth for available steric height estimates for correcting tide gauges. (Argo floats, for instance, do not operate in depths less than 2000 m.) Of course, it is equally true that obtaining steric height

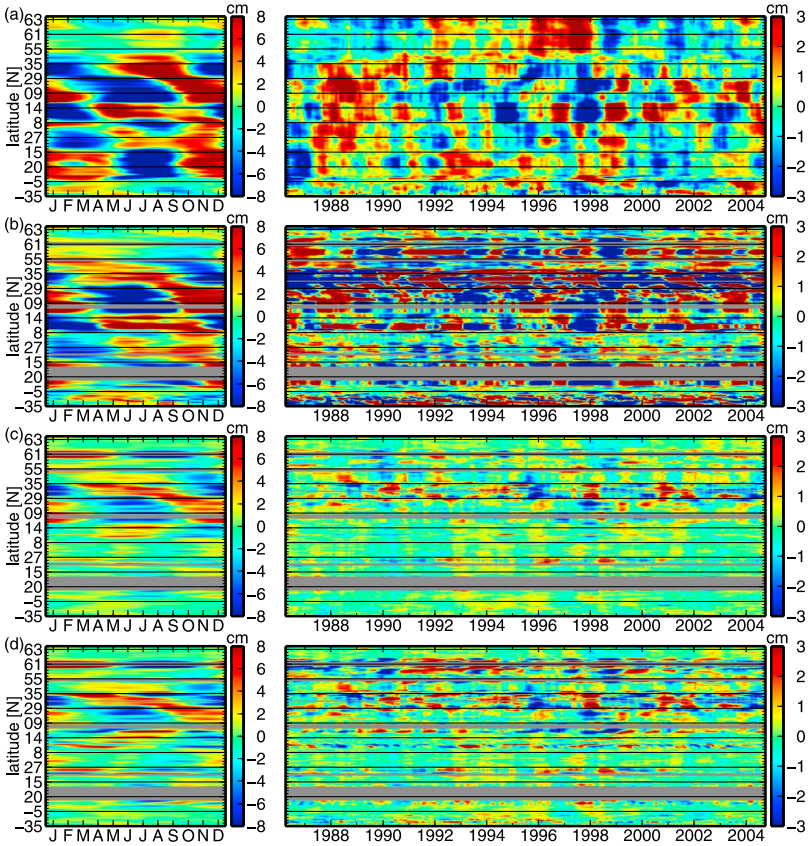

Figure 11. (a) Modeled coastal sea level variability tracing the Indian and Pacific Ocean coasts north from the southern tip of Africa. (b–d) Residuals upon subtraction from the sea level shown in Figure 11a of the reconstructions of coastal sea level under approximations A, C, and D, respectively.

information closer to shore is more feasible than measuring bottom density up the continental slope, and there may be a compromise to be made between larger bottom pressure signals in shallow water, and smaller introduced errors resulting from currents on the continental slope, shoreward of the measurement depth. Finally, therefore, we examine the impact of choice of reference level on the steric correction.

[50] As Figure 14 reveals, in most cases the steric correction can be improved by using steric height closer to the coast, with the best results obtained at 500 or 1000 m. On eastern boundaries the steric method at 500 m gives skill scores which are only marginally poorer than those obtained by the bottom density method referenced to 3000 m. The greatest difference being 13% for the southeast Pacific time series, where, compared with the northeast Pacific time series, skill increases more slowly as we move up the continental slope. The largest improvements in skill with decreasing distance from shore are found along the western boundaries. However, with the exception of the equatorial western Atlantic time series, the skill of the steric reconstructions are still substantially poorer than the bottom density reconstructions.

6. Discussion

[51] In this paper we have considered the relationship between dynamical changes in sea level and steric height in the presence of topography. A primary motivation for this has been to understand how tide gauges "see" the steric variability that dominates sea level in the ocean's interior. Since steric height is given by the depth integral of the density field, there should be very little steric height variability at tide gauge stations because they sit in very shallow water. This apparent contradiction is resolved, as students of coastal dynamics have long known, by recognizing that there is an indirect steric effect on bottom pressure.

[52] The simplest relationship between deep ocean and coastal sea level occurs in the case when there are no intervening boundary currents. In this case, it can be assumed that bottom pressure in the deep ocean is constant (we take the 3000 m contour as the starting point for the deep ocean; addition of mass to the ocean will produce a bottom pressure signal in addition to the dynamical signals considered here), so sea level changes above the 3000 m contour can be calculated simply from the variations in steric sea level at that point and, with no boundary currents, these same variations will be reflected at nearby tide gauges. This is the steric method resulting from approximation A. In this case, a warming of the ocean (for example) would result in an increase in coastal sea level and an associated increase in bottom pressure at all warmed depths. As the water is lifted when its density decreases, so the mass of water above a given depth increases (here we neglect a small decrease in deep ocean bottom pressure required to conserve mass, as the area of the deep ocean is large compared to the coastal

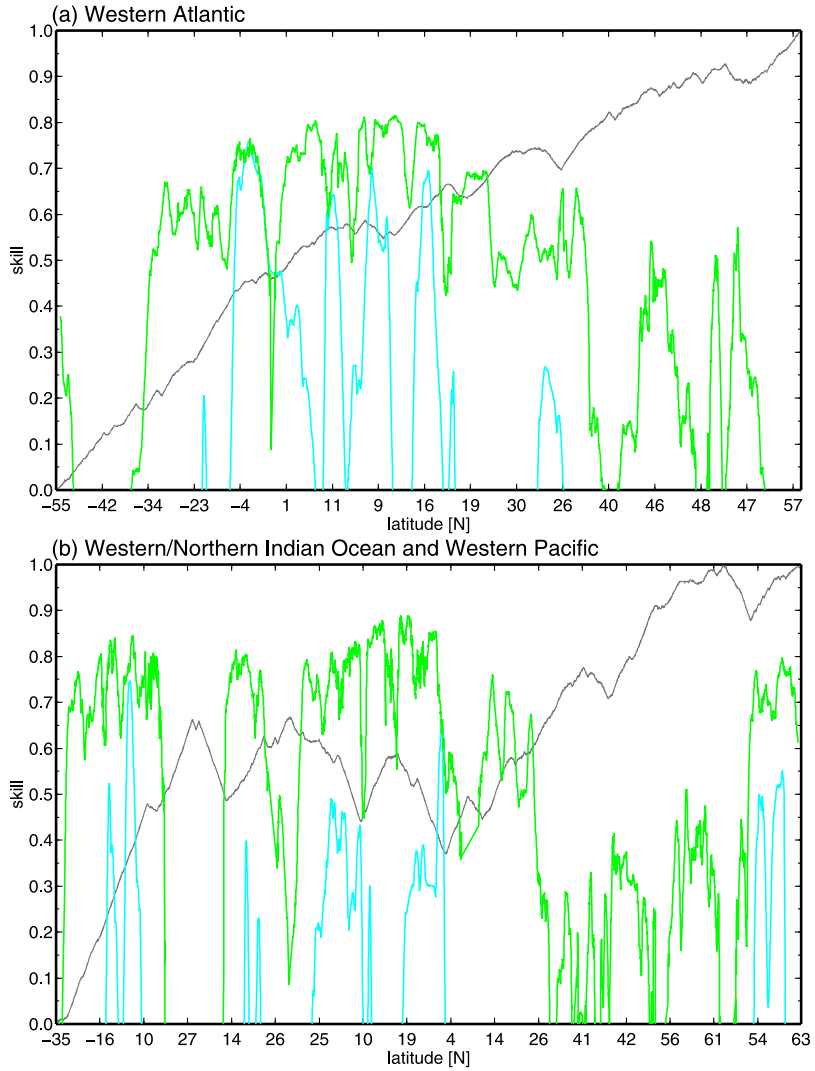

Figure 12. (a) The skill of approximations A (cyan) and C (green) in accounting for the modeled coastal sea level variability along the Atlantic western boundary. (b) The same as Figure 12a for the Indian and Pacific Ocean coasts, north from the southern tip of Africa. The grey line gives an indication of how latitude varies along the coast between the latitudes marked on the *x* axis.

region). This is essentially the picture described by *Landerer et al.* [2007] but applied locally rather than globally.

[53] For interannual variability, we find that this simple steric approximation only works well in eastern boundary regions close to the equator (Figures 6, 7, 8, 10, and 12). Elsewhere, the decoupling between sea level changes in deep and shallow water, noted by *Hughes and Williams* [2010] to occur at high frequencies, also extends to interannual variability. However, with some spatial smoothing, the steric approach also gives fairly good results at higher latitudes, particularly in the Atlantic, but again only on the eastern boundary (Figures 9 and 13).

[54] The clearest illustration of the failure of the simple assumption A, underlying the steric approach, is given in Figure 7, which shows that sea level changes on the Pacific eastern boundary are highly coherent across almost the entire latitude range (Figure 7a). While these variations are well captured by the steric method within the tropics, progressively less of the signal is captured as latitude increases, showing that the sea level signal is progressively more boundary-trapped at higher latitudes. This is suggestive of the geometry of Rossby waves which travel faster at lower latitudes, leading to smaller phase lag between coast and deep ocean, and cannot propagate poleward of a certain (frequency dependent) latitude, leading to boundary trapping of signals beyond that latitude. If this is the explanation, then we should expect the simple method to work better at lower frequencies. On western boundaries, no such argument can be made and the neglect of boundary currents is clearly inappropriate.

[55] The simple approximation A effectively assumes that there are no surface currents between the deep ocean and the tide gauge. If we accept that there will be boundary currents, we can investigate the possibility of using density information on the continental slope in other ways to (at least partially) account for these currents. This is essentially the standard hydrographer's reference level problem, and we have investigated two plausible assumptions: no geostrophic

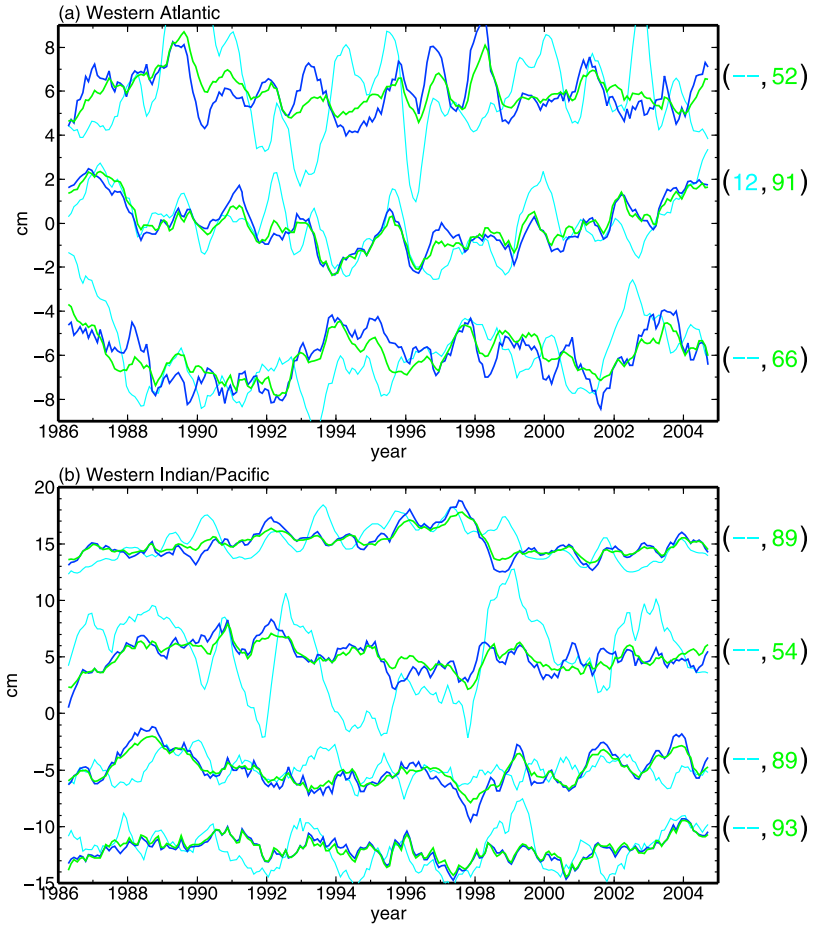

Figure 13. (a) Averages along the Atlantic western boundary of coastal sea level (blue) and sea level reconstructions based on assumption A (cyan) and assumption C (green), with averages computed over 55°S–10°S (bottom), 10°S–30°N (middle), and 37°N–50°N (top). (b) The same as Figure 13a for the Indian and Pacific western boundaries, with averages computed over 35°S–5°S along the Indian Ocean western boundary (fourth set of lines), the tip of Malaysia around the South China Sea and Yellow Sea coasts to 30°N (third set), 30°N–53°N (second set) and 53°N–63°N (first set). The skill scores for the two reconstructions are shown to the right of each along-shore mean time series in corresponding colors. Dashes represent negative skills.

current at the bottom (approximation C), and no depth-averaged geostrophic flow (approximation D). Either of these seems more likely than the assumption of no surface current, with C matching the idea of wave modes, which tend to have near nodes in bottom current over topography, and D matching the idea of linear, flat-bottom baroclinic wave modes with no depth-integrated transport. Globally, we find approximation C to be slightly, but systematically, better (Figure 4), although D is better in an equatorial band where the bottom pressure signal being modeled is typically weak (Figure 3b). Approximation C results in a correction to the simple, local steric prediction of sea level slopes, which involves the bottom density and topographic slope (making it most important in regions of steep topography such as the continental slope). It is this correction term which accounts for the influence of steric signals in the shallow water where tide gauges are located.

[56] For the purpose of providing an estimate of the steric effect at tide gauges, either of approximations C or D is significantly better than approximation A, with very little difference between C and D (Figures 6, 7, 10, and 11). On eastern boundaries, the use of approximation C improves the predictions based on A from reasonable to good (Figures 8 and 9), and on western boundaries the prediction is transformed from useless to reasonable in many places (especially with spatial averaging) and sometimes good (Figures 12 and 13).

[57] These differences illustrate the importance in many regions of obtaining density information in the small triangle of the ocean between a vertical line above the 3000 m depth contour, and the continental slope. While approximation D requires densities throughout this triangle, approximation C only requires bottom density.

[58] The residual signals which remain in Figures 6c, 6d, 7c, 7d, 10c, 10d, 11c, and 11d show that although approximations C and D represent a significant improvement, there remain signals which may be attributed to significant bottom currents, residual bottom pressure variability at the 3000 m contour, or shelf sea processes in which friction, rather than bottom currents, may play an important role in balancing pressure gradients at the seafloor. Explicit measurement of

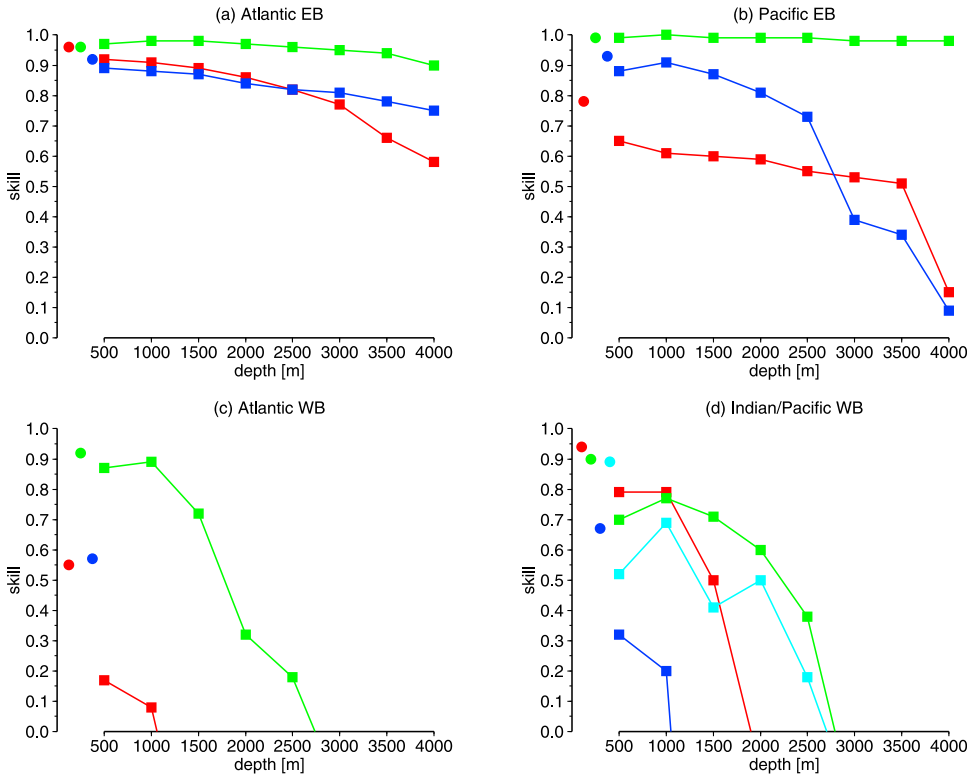

Figure 14. Testing the impact of depth (distance to shore) on the skill of the steric method (assumption A) for the along-shore average time series as defined previously: (a) The Atlantic eastern boundary, with averages computed over 35°S–5°S (red), 5°S–10°N (green), and 10°N–50°N (blue). (b) The Pacific eastern boundary, with averages over 57°S–40°S (red), 40°S–32°N (green), and 32°N–61°N (blue). (c) The Atlantic western boundary, with averages computed over 55°S–10°S (red) and 10°S–30°N (green). The skill for the interval 37°N–50°N (which would have been blue) is negative for all depths and so does not appear. (d) The Indian and Pacific western boundaries, with averages computed over 35°S–5°S along the Indian Ocean western boundary (red), the tip of Malaysia around the South China Sea and Yellow Sea coasts to 30°N (green), 30°N–53°N (blue), and 53°N–63°N (cyan). The solid circles represent the corresponding skill of the bottom density method referenced to 3000 m.

the bottom currents, in addition to bottom density, would help resolve this missed variability, particularly in western boundary regions. It is notable that the regions of least skill tend to be those with the strongest western boundary currents and/or weak stratification, which could be expected to lead to strong bottom currents.

[59] As pointed out by *Miller and Douglas* [2004], the precise position at which density measurements are made in order to provide a prediction of the steric effect at tide gauges can make a large difference to the prediction. Our results (Figure 14) confirm this for interannual variability. We find that for both eastern and western boundaries the best steric method estimates of coastal sea level are obtained within the 500–1000 m depth range. On the eastern boundaries, within this range the steric estimates are only marginally poorer than the bottom density estimates referenced to 3000 m. On the western boundaries, the bottom density method is still substantially better, with the exception of the equatorial Atlantic. While one might expect the errors in the steric method to be reduced by performing the depth integral in shallower depths, thus reducing both the size of the steric correction and the amount of boundary current between the reference location and coast, that the best steric estimates of sea level are obtained in such shallow water is, nonetheless, surprising. It illustrates how surface currents over the continental slope, especially along western boundaries and at higher latitudes on eastern boundaries, act to decouple the deep ocean and coastal sea level, such that interannual coastal sea level fluctuations are largely driven by steric variability over the upper slope. The extent to which this behavior applies at longer time scales requires further study.

7. Practical Implications

[60] We end by summarizing the findings of this paper in terms of their practical implications for interpreting tide gauge records.

[61] 1. The apparent paradox that steric corrections to tide gauges should be zero because tide gauges sit in very shallow water is resolved by recognizing, as Fritjof Nansen did in 1930 [*Helland-Hansen*, 1934], that there is an indirect steric effect on bottom pressure. This occurs even in the absence of any currents between the shelf and the deep regions where the steric signal is significant, in which case the bottom density at each depth is equal to the open ocean density at the same depth.

[62] 2. The question of how to use density information therefore revolves around how best to reconstruct these bottom pressure signals. In the absence of any information about currents, the best tactic is to assume negligible bottom current, in which case bottom density at the seafloor is the required information. Assuming a baroclinic mode structure with zero depth integral is better only in deep ocean regions near the equator.

[63] 3. In some regions, the topographic density correction is close to the conventional steric correction using a deep ocean cast, as long as that cast is onshore of any major currents. This means we can use historical measurements to produce a meaningful steric correction in these regions. Elsewhere, and particularly on western boundaries, the difference between a deep ocean cast and bottom densities on the continental slope is crucial, and bottom currents may also be important in some regions. However, in all cases interannual noise can be reduced by calculating the steric correction as close as possible to the shelf edge.

[64] 4. The importance of boundary currents in most regions shows that significant differences remain between sea level signals at the coast and those in the ocean interior, even at interannual time scales. The exception to this is on eastern boundaries in the tropics, where the decoupling is relatively small. We might expect that deep ocean to coast coupling would increase at longer time scales, but decoupling remains significant at the 3–5 year time scales which typically dominate the time series investigated here.

[65] **Acknowledgments.** This work was funded by grants from the U.K. Natural Environment Research Council. We greatly appreciate the time and effort of three anonymous reviewers, whose comments helped us improve the original manuscript, and the efforts of Andrew Coward and Beverly de Cuevas in providing the OCCAM data.

References

Bingham, R., and C. Hughes (2008), The relationship between sea-level and bottom pressure variability in an eddy permitting ocean model, *Geophys. Res. Lett.*, *35*, L03602, doi:10.1029/2007GL032662.

Cabanes, C., A. Cazenave, and C. L. Provost (2001), Sea level rise during past 40 years determined from satellite and in situ observations, *Science*, *294*(5543), 840–842, doi:10.1126/science.1063556.

Cabanes, C., T. Huck, and A. C. de Verdière (2006), Contributions of wind forcing and surface heating to interannual sea level variations in the Atlantic Ocean, *J. Phys. Oceanogr.*, *36*(9), 1739–1750, doi:10.1175/JPO2935.1.

Church, J., and N. White (2006), A 20th century acceleration in global sea-level rise, *Geophys. Res. Lett.*, *33*, L01602, doi:10.1029/2005GL024826.

Church, J., N. White, R. Coleman, K. Lambeck, and J. Mitrovica (2011), Estimates of the regional distribution of sea level rise over the 1950–2000 period, *J. Clim.*, *17*(13), 2609–2625.

Csanady, G. T. (1979), The pressure field along the western margin of the North Atlantic, *J. Geophys. Res.*, *84*(C8), 4905–4915.

Enfield, D., and J. Harris (1995), A comparative study of tropical Pacific sea surface height variability: Tide gauges versus the national meteorological center data-assimilating ocean general circulation model, 1982–1992, *J. Geophys. Res.*, *100*(C5), 8661–8675, doi:10.1029/95JC00752.

Firing, Y., M. Merrifield, T. Schroeder, and B. Qiu (2004), Interdecadal sea level fluctuations at Hawaii, *J. Phys. Oceanogr.*, *34*(11), 2514–2524, doi:10.1175/JPO2636.1.

Frankcombe, L., and H. Dijkstra (2009), Coherent multidecadal variability in North Atlantic sea level, *Geophys. Res. Lett.*, *36*, L15604, doi:10.1029/2009GL039455.

Greatbatch, R. (1994), A note on the representation of steric sea-level in models that conserve volume rather than mass, *J. Geophys. Res.*, *99*, 12,767–12,771.

Greatbatch, R. J., A. F. Fanning, A. D. Goulding, and S. Levitus (1991), A diagnosis of interpentadal circulation changes in the North Atlantic, *J. Geophys. Res.*, *96*(C12), 22,009–22,023.

Helland-Hansen, B. (1934), The Sognefjord section: Oceanographic observations in the northernmost part of the North Sea and the southern part of the Norwegian Sea, in *James Johnstone Memorial Volume*, pp. 257–274, Liverpool Univ. Press, Liverpool, U. K.

Holgate, S. J., and P. L. Woodworth (2004), Evidence for enhanced coastal sea level rise during the 1990s, *Geophys. Res. Lett.*, *31*, L07305, doi:10.1029/2004GL019626.

Hong, B., W. Sturges, and A. Clarke (2000), Sea level on the U.S. East Coast: Decadal variability caused by open ocean wind-curl forcing, *J. Phys. Oceanogr.*, *30*, 2088–2098.

Hughes, C. (2008), A form of potential vorticity equation for depth-integrated flow with a free surface, *J. Phys. Oceanogr.*, *38*, 1131–1136, doi:10.1175/2007JPO3809.1.

Hughes, C. W., and S. D. P. Williams (2010), The color of sea level: Importance of spatial variations in spectral shape for assessing the significance of trends, *J. Geophys. Res.*, *115*, C10048, doi:10.1029/2010JC006102.

Kohl, A., and D. Stammer (2008), Decadal sea level changes in the 50-year GECCO ocean synthesis, *J. Clim.*, *21*(9), 1876–1890, doi:10.1175/2007JCLI2081.1.

Landerer, F., J. H. Jungclaus, and J. Marotzke (2007), Ocean bottom pressure changes lead to a decreasing length-of-day in a warming climate, *Geophys. Res. Lett.*, *34*, L06307, doi:10.1029/2006GL029106.

Marcos, M. G. W., W. Bosch, and R. Savcenko (2007), Decadal sea level trends in the Bay of Biscay from tide gauges, GPS and TOPEX, *J. Mar. Syst.*, *68*(3–4), 529–536.

Marsh, R., B. de Cuevas, A. Coward, J. Jacquin, J.-M. Hirschi, Y. Aksenov, G. Nurser, and S. Josey (2009), Recent changes in the North Atlantic circulation simulated with eddy-permitting and eddy-resolving ocean models, *Ocean Modell.*, *28*(4), 226–239, doi:10.1016/j.ocemod.2009.02.007.

Miller, L., and B. Douglas (2004), Mass and volume contributions to twentieth-century global sea level rise, *Nature*, *428*(6981), 406–409, doi:10.1038/nature02309.

Miller, L., and B. C. Douglas (2006), On the rate and causes of twentieth century sea-level rise, *Philos. Trans. R. Soc. A*, *364*(1841), 805–820.

Myers, P. G., A. F. Fanning, and A. J. Weaver (1996), JEBAR, bottom pressure torque, and Gulf Stream separation, *J. Phys. Oceanogr.*, *26*, 671–683.

Qiu, B. (2002), Large-scale variability in the midlatitude subtropical and subpolar North Pacific Ocean: Observations and causes, *J. Phys. Oceanogr.*, *32*, 353–375.

Sheng, J., and K. R. Thompson (1996), A robust method for diagnosing regional shelf circulation from scattered density profiles, *J. Geophys. Res.*, *101*(C11), 25,647–25,659.

Sturges, W., and B. Hong (2001), Gulf Stream transport variability at periods of decades, *J. Phys. Oceanogr.*, *31*, 1304–1312.

Tokmakian, R., and J. L. McClean (2003), How realistic is the high-frequency signal of a 0.1° resolution ocean model?, *J. Geophys. Res.*, *108*(C4), 3115, doi:10.1029/2002JC001446.

Vinogradova, N., R. Ponte, and D. Stammer (2007), Relation between sea level and bottom pressure and the vertical dependence of oceanic variability, *Geophys. Res. Lett.*, *34*, L03608, doi:10.1029/2006GL028588.

Volkov, D., and H. van Aken (2003), Annual and interannual variability of sea level in the northern North Atlantic Ocean, *J. Geophys. Res.*, *108*(C6), 3204, doi:10.1029/2002JC001459.

Wenzel, M., and J. Schröter (2010), Reconstruction of regional mean sea level anomalies from tide gauges using neural networks, *J. Geophys. Res.*, *115*, C08013, doi:10.1029/2009JC005630.

Wöppelmann, G., C. Letetrel, A. Santamaria, M. Bouin, X. Collilieux, Z. Altamimi, S. Williams, and B. M. Miguez (2009), Rates of sea-level change over the past century in a geocentric reference frame, *Geophys. Res. Lett.*, *36*, L12607, doi:10.1029/2009GL038720.

R. J. Bingham, School of Civil Engineering and Geosciences, Newcastle University, Newcastle upon Tyne NE1 7RU, UK. (rory.bingham@ncl.ac.uk)

C. W. Hughes, National Oceanography Centre, Joseph Proudman Building, 6 Brownlow Street, Liverpool L3 5DA, UK.